Jestr

Journal of Engineering Science and Technology Review 15 (4) (2022) 154 - 165

JOURNAL OF
Engineering Science and Technology Review

Research Article

www.jestr.org

Predictive Framework of Conveyor Idler Bearings Fault Monitoring using Efficient Signal Processing Technique

Amritpal Kaur[1,*], Saud Altaf[2] and Sofia Iqbal[3]

[1]*School of Engineering, Auckland University of Technology, Auckland, New Zealand*
[2]*Pir Mehr Ali Shah Arid Agriculture University Rawalpindi Pakistan*
[3]*Pakistan Space & Upper Atmosphere Research Commission, Pakistan*

Received 4 April 2022; Accepted 18 August 2022

Abstract

Conveyor belts are used in many industries, from food to mining and power generation. These conveyors consist of many subsystems, and these systems, like any mechanical system, are prone to failure. The failure of these systems can cause the conveyor to be stopped and repaired, and during this downtime, production is lost. Thermal cameras are the most using method to diagnose the faults in bearing that produce the heating than the healthy bearing. Acoustic gear and accelerometer are used to capture the idler sound and vibration to detect the current health of the idler. But, these diagnosis methods need an engineering presence near the belt and monitoring purposes. However, these sensors can be monitored by only a few idlers nearby, and the installation cost of these makes the monitoring system infeasible. A predictive maintenance framework and mathematical modelling of a belt conveyor have been proposed to identify the faults before the severe damage of the belt. The experimental results showed that the in-belt monitor could identify a faulty bearing even before failure occurred. This allows all the defective bearings to be identified and the needed stock can be purchased ahead of a planned outage, and all the faulty bearings can be replaced. One large, scheduled outage can be organized to replace all defective bearings and bearings showing signs of failure soon, reducing the number of short power failures that punctuate the conveyor feed. This form of monitoring is insufficient for estimating the remaining service life of the faulty bearings.

Keywords: Conveyor belts, Signal processing, Fourier Transform, Bearing, fault Monitoring, Wavelet.

1. Introduction

Food processing, mining, and even the production of electricity all make use of conveyor belts (Yassa, 2019). These conveyors have many moving parts, and just like any other mechanical system, they can break down. The conveyor may need to be shut down and repaired if these systems fail, resulting in lost production time (Boudane, 2017).

The belt is typically one of the most expensive parts of a conveyor system. Approximately one third of the total cost of installation is attributable to the cost of the belt. When the supporting idlers become seized or have difficulty rotating, belts are more likely to become damaged (Boudane, 2017). The belt and driving unit are subjected to additional strain and stress as a result of the idlers becoming frozen. Belts degrade when they are dragged over a stationary idler, and belts have been known to tear and even rip in two, in which case the two ends of the rip need to be reattached in order to form a continuous loop again (Meshgin-Kelk, 2017). Belts have also been known to wear out over time. Belts that have been damaged can be very expensive to repair (Boudane, 2017).

Idler bearings get dirty and eventually fail, which can cause the idler to seize up (Luo, (2019).). Conveyors can range in length from a few hundred meters to several kilometers, with potentially thousands of bearings spread out along its length (Jankowska, 2022). It's possible for the bearings in any of these idlers to fail, and if the problem isn't caught in time, it can cause serious enough damage to the belt that large chunks of the belt will need to be removed and replaced (Luo, 2019).

A bearing has the fundamental frequency of the inner- outer- and rolling elements. There are numerous ways in which a bearing can fail, and these different faults can present themselves at the fundamental frequencies within the bearing (Nandi, 2017). These changes in the frequency spectrum are widely used to identify faults in bearings and other mechanical equipment. Several components in a bearing can fail, each having a different outcome on the frequency spectrum, and for this reason, different bearing fault cases will be tested on the conveyor test bench. There will be five bearing conditions:

- Healthy bearing: Since idlers have no bearing faults, it is also important to include this as one of the bearing conditions (Nandi, 2017). This also serves as a baseline to compare the faulty bearing signals. Knowing the baseline can help identify the deviations of faulty bearings, which can be used to identify better and classify faults.
- Outer raceway: Pits forming on the surfaces of bearing raceways are very common bearing faults that occur and can lead to taking failure-inner raceway (Nandi, 2017).
- Rolling element. A small pit is created on the surface of the rolling element. These pits, although small, also

*E-mail address: amritpal.kaur@aut.ac.nz
ISSN: 1791-2377
doi:10.25103/jestr.154.22

impact the raceways and can lead to similar failure (Bindu, 2018).

- Contamination: Bearings become contaminated with dust and dirt, which can lead to the acceleration of bearing failure (Fu, 2019, November). When failing bearings are replaced, it will be beneficial to know which bearings, although not damaged yet, are contaminated. Contaminated bearings may not show significant signs of failure, but one may want to replace them as a preventative measure. For this reason, bearings are contaminated with fine sand and are tested in the hope that they may also be identified and classified (Fu, 2019, November).

A method for early bearing failure detection will allow the faulty bearings to be detected before the idlers seize and start to damage the belt (Hassan, 2018). An automated idler monitoring system is desired to monitor the conditions of all the idler's bearings and notify an operator when a faulty bearing is detected (Fu, 2019, November). This system needs to be financially feasible but accurate enough to be trusted to identify any faulty bearings.

Conveyors play an important role in the operation of the mining and power generation industry (Thomson, 2016). Conveyors continuously feed the power generation plants with the needed quantities of coal over long distances (Hassanzadeh, 2019). Conveyors can deliver their payloads continuously, and the volumes can be regulated to fit the need of the process it is feeding. Conveyors play a vital role in the smooth operation of all applicable industries, and (Cruz, 2008) continuous monitoring of these conveyors ensures that they stay operational and work optimally (Thomson, 2016).

Constant exposure to the filth and dangers of a conveyor's working environment can be harmful to human health. Conveyors in factories often result in extremely loud environments, and workers also risk breathing in harmful particles (Pandarakone, 2018). The amount of time an inspector must spend in these conditions will be drastically decreased with the implementation of an automated monitoring system (Krishna, 2013).

Today, Western Sahara boasts the world's longest operating conveyor system. The combined conveyor system is just over 100 km in length and has been in operation for more than 30 years (Pandarakone, 2018). Phosphate is transported from the mines to the coast via conveyor belts; in the aerial photograph, the white line of the conveyor can be seen where some of the phosphate has been blown off. Durable rubber reinforced with steel cords is used to make belts that move heavy loads like stone, coal, and ore (Pandarakone, 2018)

By giving the belt a quarter turn on the bottom section of the conveyor, you can make it so that it wears evenly across all of its exposed surfaces, rather than just on one side, as is the case with the conveyor belts that we are used to seeing today (Tsypkin, 2017). The Turnover Conveyor Belt System was initially more sturdy than its untwisted counterparts, but the advent of modern belts that are made of multiple layers of material has rendered the twist obsolete (Tsypkin, 2017).
The most extended conveyor system in use today is in Western Sahara. The combination of conveyors has a total length of just over 100 km and has been in use for over 30 years (Pandarakone, 2018). The conveyor belts transport phosphate from the mines to the coast, and as some of the phosphates are blown from the belts, it leaves a distinct white line of the conveyor in the aerial view (Ishikawa, 2013). Belts used to transport bulk materials like stone, coal, and ore are made from rugged rubber reinforced with steel cords (Pandarakone, 2018).

Along the length of conveyors, there can be hundreds, if not thousands, of idlers. The belt is carried from one end to the other by means of these idlers. In most cases, a broken belt is caused by a faulty set of idlers (Bruno, 2015). As the bearings wear, the idler's smooth rotations are hampered, and in extreme cases, the entire idler can seize. When the bearings wear out, the idlers can't rotate freely, increasing the friction between the idler and the belt. The shell of the idler and the belt's surface both wear down due to the friction between the two. In extreme cases, the idler can completely freeze, causing the belt to drag its load over the immobile idler. There is belt damage due to the damaged and seized idlers (Al-Ahmar, 2019)
Seals are used to protect the bearings from the environment, keeping dust and mud away from the bearings to increase the usable life. Bearings contaminated with dust or dirt tend to seize or fail catastrophically (Bruno, 2015). The seizure or failure of a bearing can cause an entire idler to seize, and then it will start to scrape or rub against the belt, causing unnecessary friction on the belt (Luong, 2020). This excess friction places additional strain on the power unit, and the belt may also rip, tear, or catch fire under these excessive friction forces, leading to the standstill of the conveyor.

The rest of the paper is organized into four sections: section (2) discusses different causes of conveyor belt failure, focusing on idler failure. Section (3) consists of a predictive maintenance framework and mathematical modelling of the belt conveyor. The following section (4) discusses the development of an in-belt idler monitoring system and test-bed environment. Finally, the following sections will show this paper's different results and conclusion.

2. Possible failures in a conveyor belt

Like every mechanical system, something is bound to wear and fail at some stage during the operation of the conveyor. There are plenty of individual components that make up a conveyor system, and each one of them can fail or lead to subsystems failing (Herndler, 2011). The conveyor can still operate and deliver the payload even when certain components fail - like the idlers (Jankowska, 2022). If these components are not fixed, they can lead to the failure of subsystems or other components critical to the conveyor's operation - like the belt.

The bearings in the drive unit, head and tail pulleys are subjected to enormous stresses. The bearings can fail and lead to catastrophic failure of the conveyor. Reports show that the bearings became so hot that the grease inside caught fire (Herndler, 2011). The gears inside the drive unit are also under large cyclic loads. Various condition monitoring methods have been implemented on these critical components for preventative maintenance against catastrophic failure (Pereira, 2009).

The belt of the conveyor system is an expensive component (Cruz, 2008). For nylon or polyester embedded belts, the cost of the belt is about one third the installation cost of the entire system and can be even more expensive if the belt is reinforced with a steel cord (Herndler, 2011). The cost of maintenance can be reduced by avoiding belt damage. There are a few ways to mess up the belt (Yetgin, 2019). A belt's supporting structure, or carcass, can weaken

if it is subjected to excessive stress, such as when heavy rocks are placed on the belt or when material accumulates on the idlers (Pandarakone, 2018). These defects increase the risk of the belt tearing or even breaking. For the conveyor to stop so the belt can be reattached or repaired,

Along the length of conveyors, there can be hundreds, if not thousands, of idlers. The belt is carried from one end to the other by means of these idlers. In most cases, a broken belt is caused by a faulty set of idlers (Pandarakone, 2018). As the bearings wear, the idler's smooth rotations are hampered, and in extreme cases, the entire idler can seize. When the bearings wear out, the idlers can't rotate freely, increasing the friction between the idler and the belt. The shell of the idler and the belt's surface both wear down due to the friction between the two. In extreme cases, the idler can completely freeze, causing the belt to drag its load over the immobile idler. There is belt damage due to the damaged and seized idlers (Thomson, 2016).

Although the idlers are not as complex as the drive unit, the head and tail pulley or the tensioning mechanism, they are crucial to a conveyor's smooth operation. There is a very large number of idlers along the length of a conveyor (Ishikawa, 2013). For general engineering practice, the spacing, in imperial units, of the idlers based on the belt width and the payload weight can be found in (Table 1). The table was found in an idler selection procedure (Navarro, 2020) Note the table is in imperial units.

According to the data in the Table 1, the number of idler-assemblies required per kilometre ranges from 925 to 2,049, with the exact number requiring knowledge of both the belt width and the payload mass. (Xu, 2020). Three top idlers form a trough to support the payload, while one or two bottom idlers hold up the empty returning belt in each idler assembly (Krishna, 2013). It is assumed that each assembly has four idlers, or eight bearings, with three on top supporting the payload and one on the bottom supporting the empty returning belt (Xu, 2020). That ranges from 7,400 to 16,392 bearings per km. In the mining and power generation industries, it's not uncommon for conveyors to stretch for several kilometers. Any one of those bearings could fail, causing serious damage to the belt, so careful inspection and monitoring are essential (Ishikawa, 2013).

Table 1. Suggested idler spacing (feet) in engineering practice (Navarro, 2020)

Belt width [inch]	**Number of toughing Idlers Weight of Material Handled, [Lbs. Per Cu. Ft]**						**Number of return Idlers**
	30	**50**	**75**	**100**	**150**	**200**	
14	5.5	5.0	5.0	5.0	4.5	4.5	10.0
16	5.5	5.0	5.0	5.0	4.5	4.5	10.0
18	5.5	5.0	5.0	5.0	4.5	4.5	10.0
20	5.5	5.0	5.0	5.0	4.5	4.5	10.0
24	5.0	4.5	4.5	4.0	4.0	4.0	10.0
30	5.0	4.5	4.5	4.0	4.0	4.0	10.0
36	5.0	4.5	4.0	4.0	3.5	3.5	10.0
42	4.5	4.5	4.0	3.5	3.0	3.0	10.0
48	4.5	4.0	4.0	3.5	3.0	3.0	10.0
54	4.5	4.0	3.5	3.5	3.0	3.0	10.0
60	4.0	4.0	3.5	3.0	3.0	3.0	10.0
66	4.0	4.0	3.5	3.0	3.0	3.0	10.0
72	4.0	3.5	3.5	3.0	2.5	2.5	8.0
84	3.5	3.5	3.0	2.5	2.5	2.0	8.0
96	3.5	3.5	3.0	2.5	2.0	2.0	8.0

Subsystems that do not require constant human involvement or assistance, such as the drive unit, head and tail pulley, and even the belt surface and internal structure, are monitored using a variety of condition monitoring systems (Misra, 2015). When a problem is detected, the system automatically notifies a human operator. A system is required to monitor all of the idler bearings and alert an operator of any possible failures, just as is the case with the other subsystems in the conveyor. A feasibility study conducted by Eskom indicates the need for a system to keep tabs on the conveyor belts' idlers (Misra, 2015) though it must be economically viable. The cost of the monitoring equipment must be reasonable, and workers who check on and swap out the idlers should be compensated fairly.

3. Framework For Condition-Based Maintenance And Computational Mathematics Of Belt Conveyor

Idlers' condition monitoring on a belt conveyor is assumed to involve timely roller detection, decision making, and a subsequent assessment interval. Here, a framework is proposed for fault preservation in belt conveyors, and Figure (1) provides an illustration of its application toward the system's accurate predictive maintenance. The proposed framework consists of different phases starting from real-time capturing belt features, throughput, and the belt material specifications from the instrumental system used for monitoring the input data for identifying the number of bearing failures and Current conditions of roller bearings and conveyor belt (Al-Hashedi, 2021). The output from the framework showed the idler roller and bearing failure mode for in-service inspection by engineers.

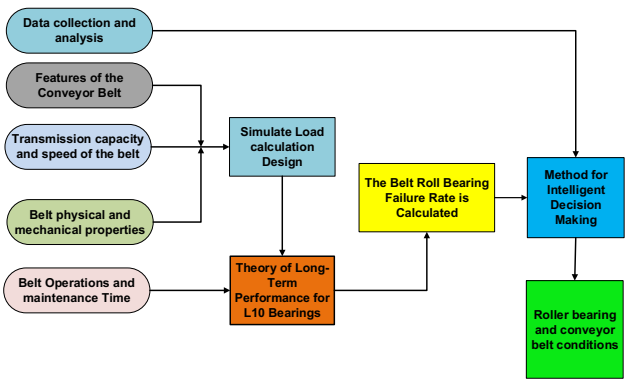

Fig. 1. Proposed framework of Decision-making structure for Maintenance the belt.

There are relationships between the algorithm, reliability, and the amount of working time that has already been attained. These relationships are necessary for the calculation of the failure percentage, which takes into account the population of identical bearings operating under the same symptoms (Refer to Equation (1) in (Hui, 2017). The accumulated density function for the failure of the roll bearings is depicted in Equation (1);

$$Failure_{tc}(T) = 1 - B_R(T) = 1 - exp\left(-0.1053\left(\frac{(L_s(T))}{L_{10,m}}\right)^{10/9}\right) \quad (1)$$

Where $Failure_{tc}(T)$ is failure time in specific time; $B_R$is the rate of bearing; $L_{10,m}$ is the L_{10}rating life of idlers roll bearing, and the length of operational time (Hui, 2017).
The value of $L_s(T)$ can be calculated as follows in Equation (2);

$$L_s(T) = \sum_{i=1}^{N}\left(\frac{RF_i}{RF_m}\right)^3 t_i \quad (2)$$

Where $RF_i$is the radial force to $i^{th}$the level of throughput of belt conveyor on a central bearing point; t_i is the sum-up of the operational time at $i^{th}$the level of throughput; $RF_m$is the radial force value to features and material of design capacity of belt (Hui, 2017).

Furthermore, an error calculation term $\varepsilon(T)$is presented in the hypothetical calculation of failure percentage occurrence between two following assessments of idler bearings T_i. So, the failure ratio can be calculated from Equation (3) as follows (Yetgin, 2019):

$$Failure_{tc}(T_i) = \int_{t_i-1}^{i} Failure_{tc}(T_i)dt + \varepsilon(T_{i-1}) \quad (3)$$

From substituting Equation (1) into Equation (4), the constant throughput is formatted as follows for belt velocity,

$$Failure_{tc}(T_i) = exp\left(-0.01\left(\frac{L_s(T_{i-1})}{L_{10,m}}\right)^{\frac{10}{9}}\right) - exp\left(-0.01\left(\frac{L_s(T_i)}{L_{10,m}}\right)^{\frac{10}{9}}\right) \quad (4)$$

With the recognition of impreciseness of conventional L_{10}bearing fault and lifetime calculation (Equation (7) in []) is presented in our framework to modify the imprecision of consistency estimation of error term $\varepsilon(T)$ as follows in Equation (5) (Chen, 2010, March).

$$Failure_{tc}(T_i) = \int_{TH(T-1)}^{+\infty} f_{ti}(x)\,dt \quad (5)$$

Where, $f_{ti}(x)$ is the current belt monitoring frequency value relative to the time T_i.

4. In-Belt Idler Monitoring System

For very early fault detection, one can focus on the first stage of bearing failure. Monitoring the ultrasonic vibrations will give a very early insight into a bearing's health. Due to the high frequency range being measured, the sensors and data acquisition equipment required to do so are typically dearer. More readily available equipment can measure at the lower frequencies and monitor the bearing fault or defect frequencies. This will be more financially viable but will only indicate later stage failure. Faulty idlers will be replaced when it is in the later stages of failure as it makes no sense to replace a bearing when there is still significant life left. It would be beneficial to identify a faulty bearing when it is in the initial stages of failure, but identifying the bearing in the third stage of failure should give the operators enough time to evaluate the severity of the failing bearing.
Before starting the experiments, the inherent risks posed by this effect were tested with a simple experiment. This was done to see if the vibrations could be measured through all the elastomeric belt at varying distances from the starting point.

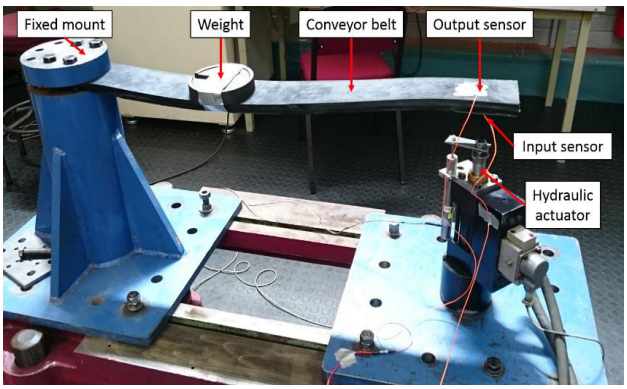

Fig. 2. Transmissibility test bench.

Figure 2 depicts the experiment conducted on a modest scale to explore the transmissibility of the fault. The significant components are labelled in the Figure:

- The tremor was generated by a hydraulic actuator. A range of 0-1000 Hz was scanned for frequencies. Because failure occurs at these lower frequencies only in the later stages, it is more important to characterize them accurately than higher or ultrasonic frequencies.
- An accelerometer was used to measure the vibration signal generated from the hydraulic actuator. The input sensor was fixed to the underside of the belt on its centerline, where the hydraulic actuator connected to the belt. This represented the source of the vibrations that are induced by the idler.
- The belt's central line above the sensor's output was used to measure vibrations. The sensor for the practical application should go here. We started by putting the sensor right where it would be needed, over the origin and backed off the light with every fifty millimeters. This was accomplished as far as 400mm from the origin and the typical distance between two idlers is 800 mm. The sensors will assign the measured signal to the next idler when it's halfway between the two. This is why tests were limited to 400mm.
- The effects of a load on the belt were crudely simulated by adding weight to the system. As a result of the uneven distribution of force, the concentrated weight was not representative of typical loads. Simply to the left of the farthest measuring point is where the weight was positioned. The belt was attached at one end to a stationary pole. Free belt length measured 800mm.
- The conveyor belt used is a sample cut from a steel cord reinforced rubber belt. Fenner produces this belt for the materials handling industry. This industry is where this

monitoring method is aimed, and this type of belt will be used in the tests for this reason.

The transmissibility at a certain distance from the sourcewas calculated by comparing the input or source vibration to the measured output vibration. The time signals of both accelerometers were analyzed in the frequency domain. A Fast Fourier transform (FFT) was done on the measured signals. The two sensors were connected to the same data logger so that both signs had the same sampling frequency. Each value of the two signals that corresponded to the same frequency was used to determine the transmissibility in the frequency domain

The transmissibility for the entire frequency range and all nine measured distances was calculated. Figure 3 shows the gradient filled contour plot of the transmissibility of vibrations through the belt.

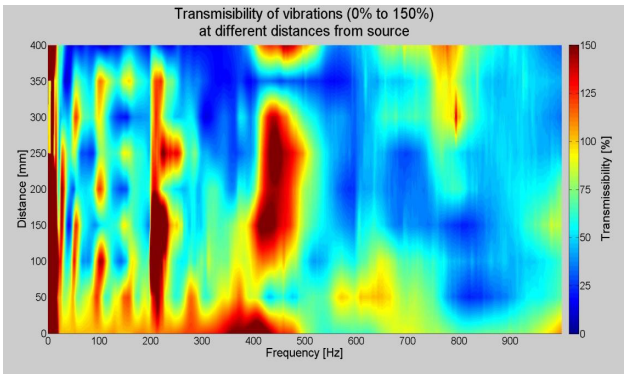

Fig. 3. Transmissibility of vibrations through the belt.

As seen in Figure 3, the transmissibility of the vibrations is very good, close to the source for a wide range of frequencies. In the region on the belt from 0mm to 50mm and at a frequency of 0 Hz to 500 Hz, there is a yellow-orange and red region, which corresponds to 100% transmissibility and higher. The sensor is still close enough to the source that the dynamics of the belt does not influence the transmissibility too much. At higher frequencies, the transmissibility reduces quite dramatically. It is also seen that at some positions on the belt, transmissibility is more significant than 100% - red regions. This can be due to the belt resonating at its natural frequencies. The resonating belt can help amplify the underlying bearing frequencies if the bearing frequencies correspond with the belt's natural frequencies and these induced vibrations are large enough to excite the belt. However, sections of the belt attenuate the source vibrations - blue and green sections. If a sensor is measuring these regions at those frequencies, the bearing vibrations may be difficult to capture.

Referring to Figure 4, which only shows the regions with the transmissibility of 75% and higher, it can be seen that up to 50mm away from the source, the transmissibility of vibrations up to 400Hz is well above 75%. This region, indicated with the bounding box, has transmissibility of 100% and higher. It is comforting to know that sensor reading in this region will not be attenuated close to the source when tests are done on the moving conveyor.

Figure 5 shows the regions that have transmissibility of 50% and higher. It is shown that at a distance of 100mm, the transmissibility is higher than 50% for vibrations up to about 760Hz. The transmissibility is also well above 50% for frequencies up to 280Hz for distances up to 300mm away from the source. Still, sections within this range show the transmissibility below 50% - shown as the white voids in the contour plot. This is due to the mode shapes of the belt at different frequencies that have an attenuating effect on the transmissibility.

The belt has mode shapes at some frequencies where troughs and peaks in the wave magnitude can be seen in the abovementioned figures. These mode shapes change as the frequencies do and explain why, at some frequencies, the transmissibility can be very high at some point on the belt and be very low just a short distance away.

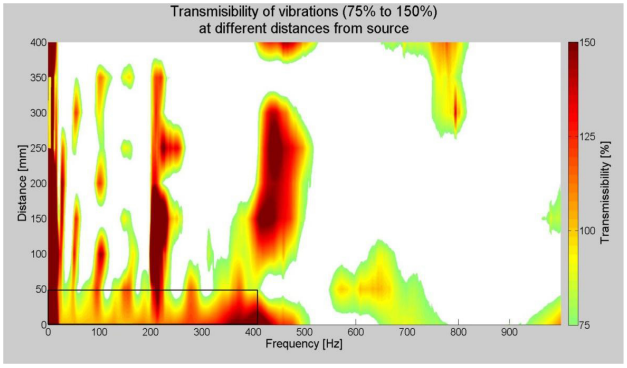

Fig. 4. 75% Transmissibility and higher.

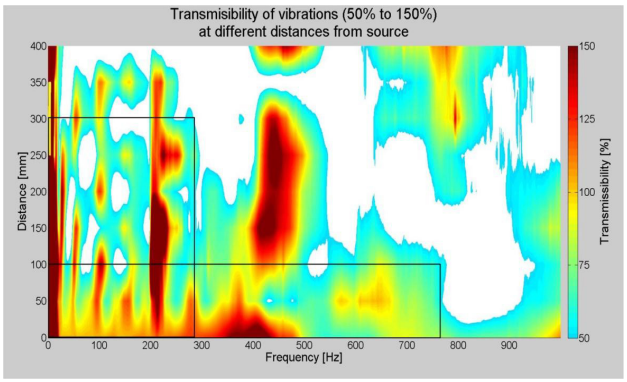

Fig. 5. 50% Transmission rate or higher.

Take 150Hz in as an example; at 50mm, 150mm, 250mm and 350mm, the transmissibility is below 100% (yellow-orange region) but can be as low as 25% or even in between lower (dark blue). From the contour plots, it can be seen that the vibrations are, as expected, attenuated more at high frequencies far from the source.

This experiment was done to investigate the magnitude of the attenuation effect of the steel-reinforced rubber belt on a vibration signal, possibly from an idler bearing, and what influence it would have on the capabilities of measuring said signal. From the experiment, it can be expected that the vibration signals from an idler bearing can be measured with little loss to the signal strength, close to the source over a wide range of frequencies, and still clearly at low frequencies far from the source. The measuring equipment should measure bearing vibrations as it approaches the idler and even as it passes and moves away. The next concern is measuring the bearing vibrations as the sensor moves towards and away from the idler. A conveyor test bench was built to investigate this (Yassa, 2019).

5. Process For Gathering Information

Conveyor idler vibrations were tracked using a custom-built data logger. A prototype was built with a 16 MHz Arduino Micro and the sampling rates were as high as 600 Hz with

12-bit resolution up to a ± 16g range. A new data logger was built with a microcontroller to improve on the specifications. The data logger reached sampling frequencies of up to 1 kHz with 16-bit resolution up to a range of ±16g. The logger has a built-in anti-aliasing filter.

The Arduino reads the accelerometer's data, writes it to a micro SD card, and transmits it via Bluetooth. Accelerometer data and a timestamp can be recorded on an SD micro card (up to 64 Gb) with the help of the logger's SD card module. The Bluetooth capabilities allow the data to be streamed live over 10m away. The Bluetooth also allows for settings to be changed without connecting a laptop to the logger. The filename and the acceleration range can be set, and the live stream capabilities can be toggled on or off with a cell phone and a serial communication application. A sampling frequency of 1 kHz is achieved if the live stream is switched off. The settings are text-based and can be changed easily with any Bluetooth enabled device. The data logger has a 2000 mAh Lithium-polymer battery built-in. This enables continuous data logging for over 50 hours. The battery can be charged with a cell phone charger. A protective aluminum case was machined to protect all the components within, and a Perspex cover allows the status indicator lights to be still visible. The overall cost of this data logger is under R2000. This is considerably less than the cost of a DTS Slice Micro and should be more financially feasible.

An LSM6DS33 accelerometer was used, which came in a separate system package. It is an accelerometer and a gyroscope with three degrees of freedom, each on a separate microchip that is smaller than 23mm x 14mm x 2.5mm and costs less than R300. Using an Inter-Integrated Circuit protocol, the data logger can communicate with the accelerometer. The sensor has a 16-bit resolution and can measure up to 16g at a frequency of up to 6.6 kHz. The sampling frequency is limited to around 1 kHz by the microcontroller and the combination of all other components and features.

6. Sample Data Preparation

Bearing problems manifest themselves in a frequency analysis at varying rates. Idler bearings have a few potential weak points. The inner and outer ring, or raceway, of the bearing can crack or pit, leading to the failure of the bearing. The rolling element, whether it's a ball or roller bearing, can pit and can cause damage to the inner and outer raceways, leading to the failure of the bearing. There is a correlation between the frequency of failure and the type of bearing element it is. As a fault progresses, the magnitude of the associated frequency is expected to increase. It is challenging to identify any obvious changes or differences in the signals. Intelligent systems (or artificial intelligence as it is also known) are widely used to recognize a change in these features that might indicate a faulty idler or any other potential faults within the bearing. These intelligent systems are used to see that, when trained correctly, they can be very accurate and consistent in identifying and classifying features like those associated with faulty bearings. The accelerometer data is first pre-processed to extract the bearing features to be used to identify and classify the bearing condition.

7. Features Extracting From Each Idler's Signal

The accelerometer continuously measures vibrations as it travels over the idler and around the pulleys. When the sensor is in the vicinity of the idler, it captures the vibrations of the bearings in the idler better than when it is at a distance from the idler. Extracting the section of the signal when the sensor is close to the idler and examining it should produce better and more precise results.

Figure 6 shows the vibration signal measured for multiple sensors passes over the idler. The sensor measures the gravitational acceleration of the Earth, which is why the signal has a *+1g* offset when the sensor is on the top part of the conveyor. A *-1g* offset when the sensor is upside down when it is on the bottom of the conveyor. This swing between the returning and the forward passes is used as a trigger because that is when the sensor moves to the top of the conveyor and is in the proximity of the idler. A moving average is applied to the signal, and a trigger value on the rising and falling edge is used to extract the portion of the signal close to the idler.

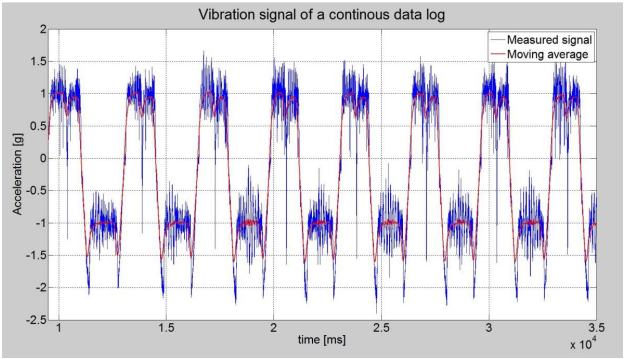

Fig. 6. Vibration signal of multiple idler passes.

Figure 7 shows an extracted signal of a single idler pass. With the triggers, the section of the vibration signal is removed when the sensor is on top of the belt and close to the bearing. The signal used to identify the underlying bearing frequencies is extracted from halfway between the tail pulley and the idler to halfway between the idler and the driven pulley. This is done so that the bearing signal extraction is done after the dynamics between the belt and pulley have had enough time to die out and before the approaching pulley affects the signal. The extracted signal should contain the bearing vibrations with minimal inclusions of the other components in the system. This section of the vibration signal that includes the bearing signal will be used, after some pre-processing, by artificial intelligence to identify and classify the bearing condition. Each pass of the idler will be used as a separate dataset. The large spike in the middle of the signal is caused by the sudden change in the vertical direction of the sensor as it passes the idler - negative vertical acceleration.

A noticeable belt hop is present between the pulleys and the idler and can be seen as the higher amplitude waves in the signal. The belt hop is included in the plain bearing signal. Still, it is at a much higher frequency than the fundamental bearing fault and should not influence the frequencies that are important for identifying the bearing conditions.

Together with the acceleration, the timestamp of each data point is also logged. The time between each data point is not the same but may differ by a few microseconds. This is caused by the microcontroller sending a request to the

sensor for its acceleration data and waiting for a response with the value. This happens hundreds of times a second, and small-time differences do occur. All the data sets have been sampled under, but close to, 1000 Hz. All the data sets have been resampled with software to 1024 Hz to keep it constant over the entire data range. Because all the data samples are resampling to the same frequency, they can be analyzed in the frequency domain with the same sampling frequency throughout.

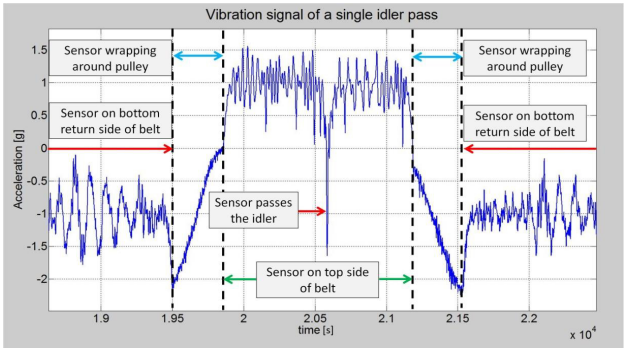

Fig. 7. Vibration signal of a single Idler pass.

It is easier to identify the underlying frequencies of a time signal by using a Fourier Transform (FT). The underlying frequencies can be determined and used to analyze the different bearing elements' health with a Fourier transform of the time signal. As each idler is monitored on its own, each idler's signal needs to be analyzed. A time-domain localization can be used to focus on each idler individually. A Short-Time Fourier Transform (STFT) can be used, seeing that a small window of the signal is analyzed at a time with a Fourier transform. This has a limited frequency resolution as a fixed window size is used. The window size can be changed, but it is fixed for the entire signal.

A method that uses variable sized windows is called a wavelet transform (WT) and has been used successfully to process bearing frequencies for fault identification and classifying. This is a more flexible method for representing a signal in the time-frequency domain. Long time windows are used to get a more acceptable low-frequency resolution, and a short time window is used to get high-frequency information. Precise frequency information at both low- and high frequencies can be obtained using wavelet transforms, making it ideal for analyzing irregular data patterns.

A wavelet package decomposition is performed on all the bearing time domain data sets using quadrature mirror filters as low- and high-pass filters. These filters have been used before with success to process bearing frequencies for fault identification and classifying.

Two decompositions of the signal are obtained by applying a level 1 wavelet decomposition on the signal. These two decomposed signals are in the time domain, but one contains the low- and the other the high-frequency components of the signal. The low-frequency component of the signal is known as the approximation, and the high-frequency component is known as the detail. Following Figure 8 shows the level 1 wavelet decomposition on a bearing signal.

A level 2 wavelet package decomposition is where the approximation (low-frequencies) and the detail (high-frequencies) signals of the first level of the decomposition are decomposed again. Now the original signal can be decomposed into four signals. Figure 9 shows the level 2 wavelet decomposition done on a bearing signal.

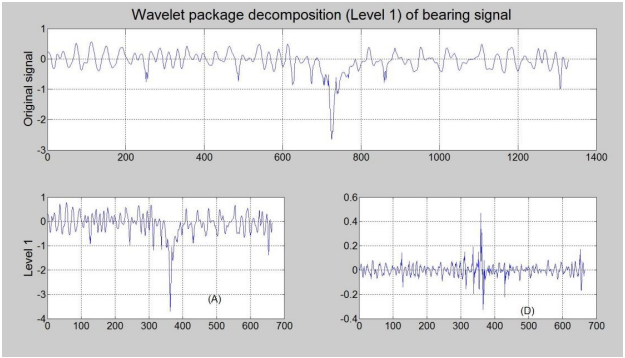

Fig. 8. Wavelet package decomposition at Level 1.

Higher-level wavelet package decompositions can be done on the original signal. Figure 10 shows a level 3 wavelet package decomposition done on a bearing signal. The higher level decompositions divide the original signal into more signals that distinguish the base signal and the underlying vibration signals even better from one another.

If the different fundamental bearing frequencies can be captured in their frequency bands, it should ease identifying and classifying the bearing faults. For this reason, it was decided to apply a level 7 wavelet package decomposition as it should capture small-signal wavelets, small enough to capture each fundamental fault frequency in its wavelet.

Frequency analysis is done on each wavelet to determine the underlying frequency data.

It will be challenging to use all the data points of the entire frequency spectrum of all the wavelet packages as inputs for the intelligent system as there will be too much. An energy value representing each of the wavelets' frequency spectrums is calculated to reduce the number of inputs to the intelligent system. By using the energy values of the wavelets, the number of information for the intelligent systems is reduced. However, the energy values are still good representations of the frequency spectrum that, in essence, build up the original signal.

8. Experimental Results

The inner raceway was fixed, and a belt speed of *1m/s* was maintained with as few variations as possible throughout the test using a variable speed drive. The idler speed was monitored as well with a hand-held tachometer. Figure 11 shows the fast Fourier transform, or FFT, of a vibration signal measured with the accelerometer when both bearings in the idler were healthy. The three fundamental frequencies are also indicated in the Figure. The fundamental frequency produced by the outer raceway was calculated to be 18.97 Hz and was measured on the FFT to be 18.63 Hz, a 1.8% difference. The fundamental frequency corresponding to the inner raceway was calculated as 27.68 Hz and measured at 26.79 Hz, a 3.2% difference. The fundamental frequency of the rolling element was calculated as 48.51 Hz and was measured at 47.63 Hz, a 1.8% difference. From this, it can be seen that the accelerometer measured vibration signals produced by the bearing that corresponded to the calculated fundamental frequencies. A total of 16 vibration signals were measured of a healthy bearing in the idler.

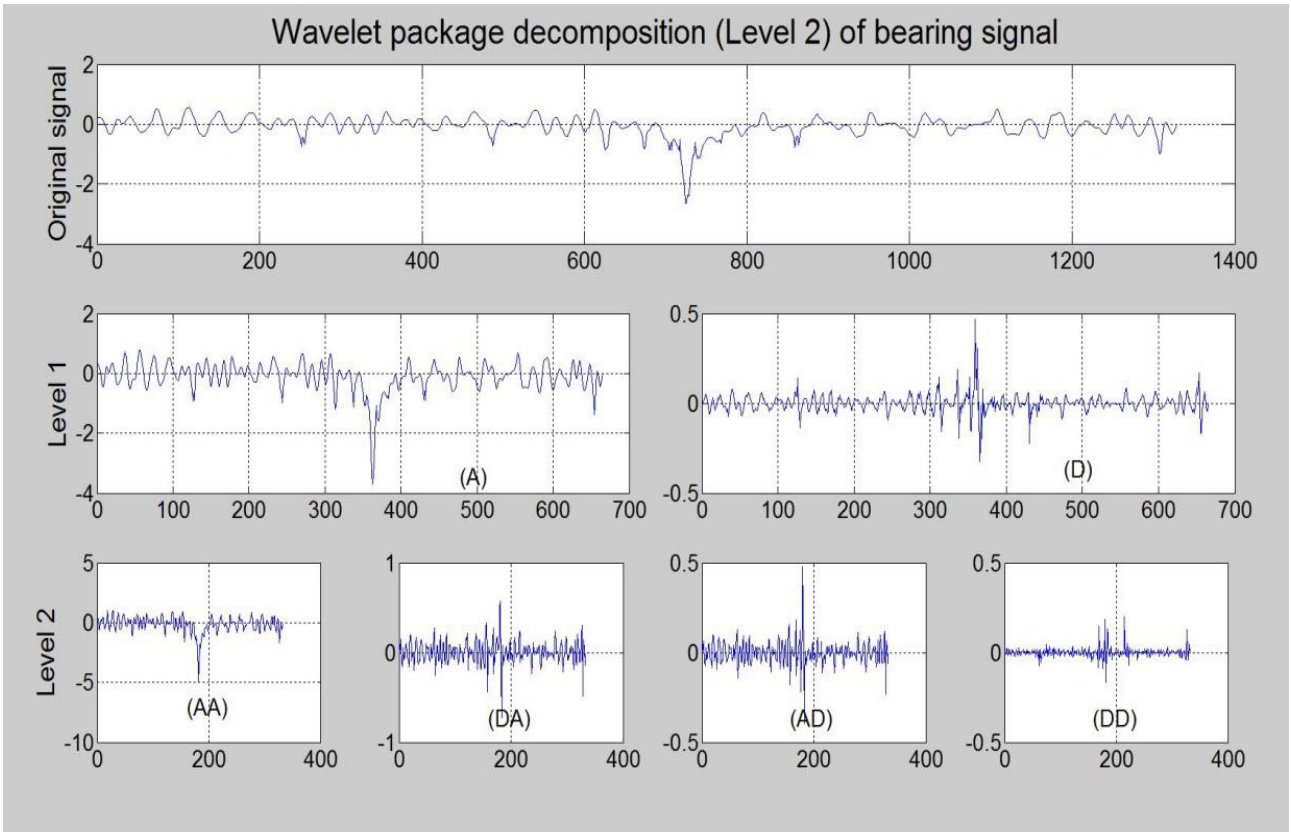

Fig. 9. Bearing signal at level 2 using WPD.

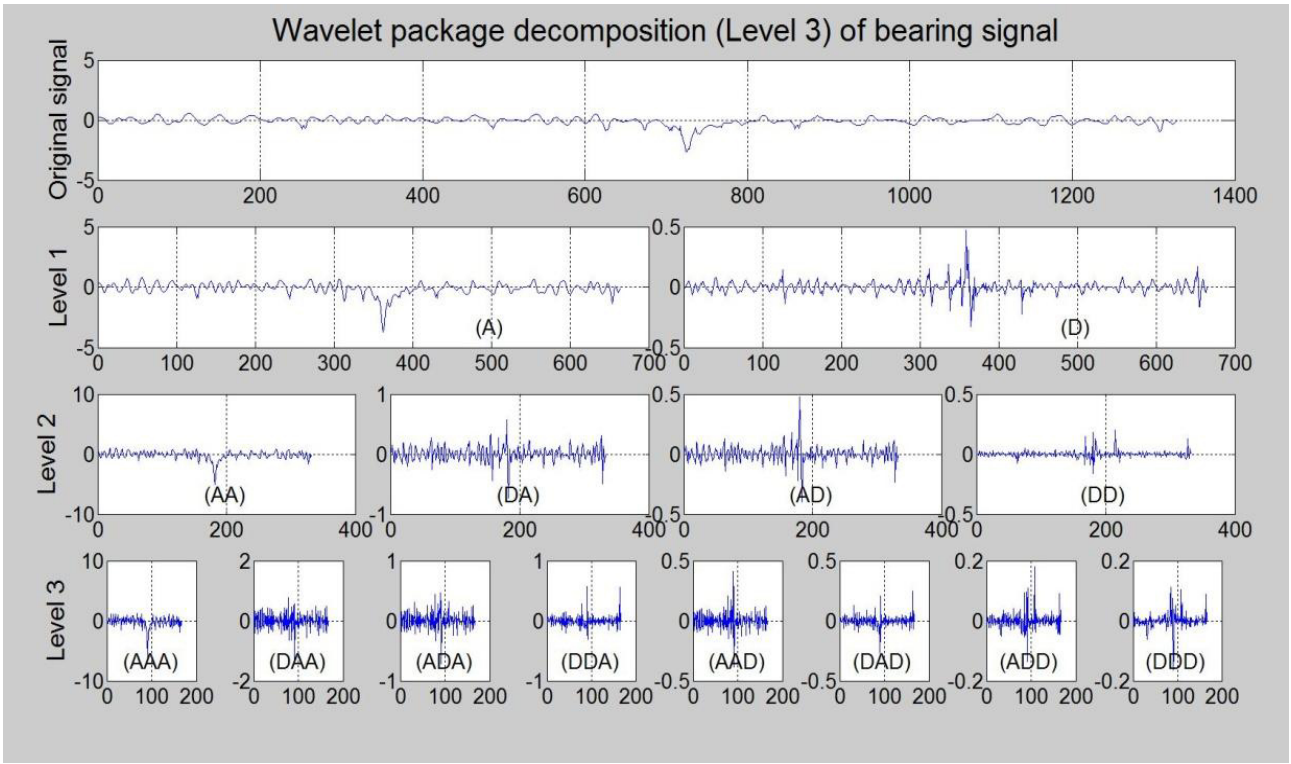

Fig. 10. Bearing signal at level 3 using WPD.

A bearing with an inner raceway defect was installed into the idler, and the accelerometer was fixed to the shaft closest to the faulty bearing. Figure 12 shows the FFT comparison of the healthy bearing and the bearing with an inner raceway fault. The moving average of the FFT is also used and is also shown. Only five data points before and five data points were used to calculate the moving average as it still kept the general shape of the frequency spectrum.

As the rolling element impacted the inner race fault, it increased the magnitude of the inner raceway fundamental frequency in the frequency spectrum - it impacted the fault at that specific frequency. A total of 12 datasets were

measured on the shaft of the idler when a bearing with an inner raceway defect was installed.

A bearing with an outer raceway defect was installed into the idler where the previous faulty bearing was. The accelerometer was fixed to the shaft closest to the faulty bearing. Figure 13 shows the FFT comparison of the healthy bearing and the bearing with an outer raceway fault. The moving averages of the FFTs are also used and are also shown. The same moving average was used throughout all the tests; only five data points before and five data points were used to calculate the moving average.

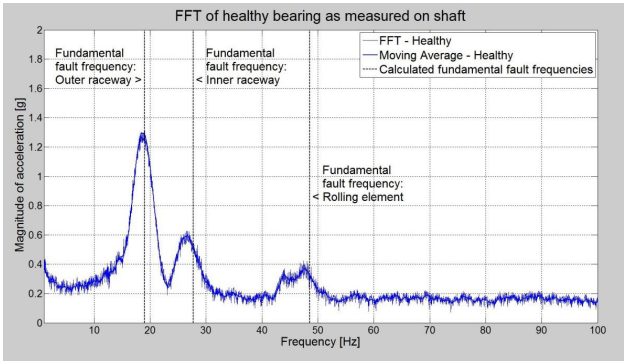

Fig. 11. *On the shaft, the FFT of a healthy bearing was measured.*

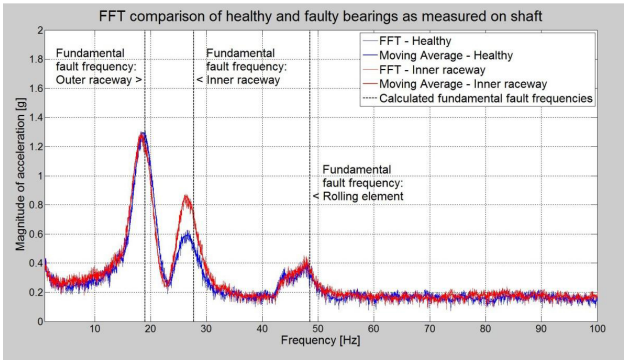

Fig. 12. Shaft FFT of an inner raceway fault.

The evaluation of the intrinsic raceway failure predicted that the fundamental frequency of the outer raceway would increase in magnitude. The frequency associated with the bearing fault increased in magnitude, but not in frequency, as it did when the internal raceway deficiency was introduced. The force of the bearing surfaces on the faulty bearing can be paired with this growth at the same rate. With only a small margin of error, the calculated fault frequency bands matched the evaluated basic frequencies of the signals. When a defective bearing was placed on the idler's shaft, fourteen sets of measurements were taken.

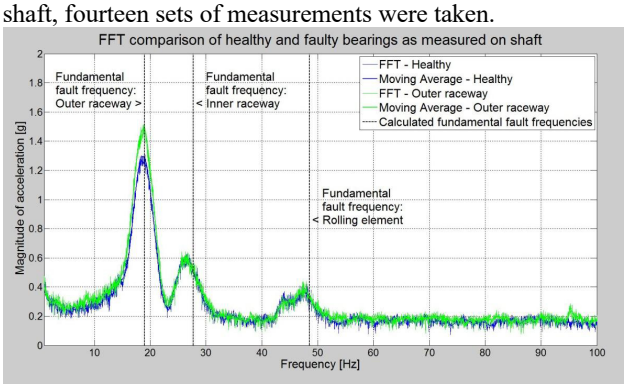

Fig. 13. Displacement FFT of a shaft-mounted outer raceway fault.

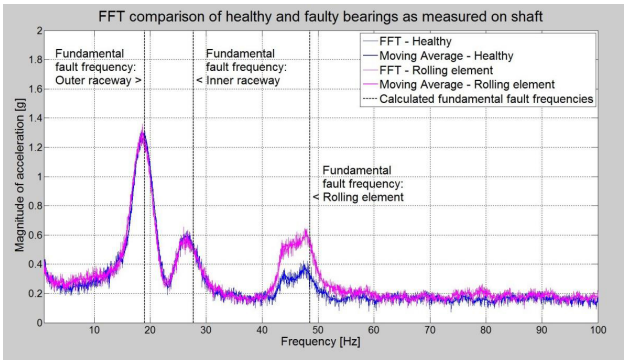

Fig. 14. Measured FFT of a fault in a rolling element taken from the shaft.

Instead of replacing the idler's original bearing, which had a flaw in its outer raceway, a new bearing with a defect in its rolling element was installed. The accelerometer was fastened onto the shaft near the failed bearing. In Figure 14, we can see an FFT comparison between a normal bearing and a bearing with a fault in its rolling element. The FFTs' moving averages are also employed and displayed. The idler now has a tainted bearing in the same spot as the faulty bearing, which was caused by a faulty rolling element. The accelerometer was fastened onto the shaft near the failed bearing. FFT analysis of a healthy and tainted bearing is displayed in Figure 15. The FFTs' moving averages are also employed and displayed.

To better understand the differences between the signals, we present a typical moving average of each of the five bearing conditions in Figure 16. The frequency spectrums of various bearing conditions differ from one another. They helped differentiate between different medical states

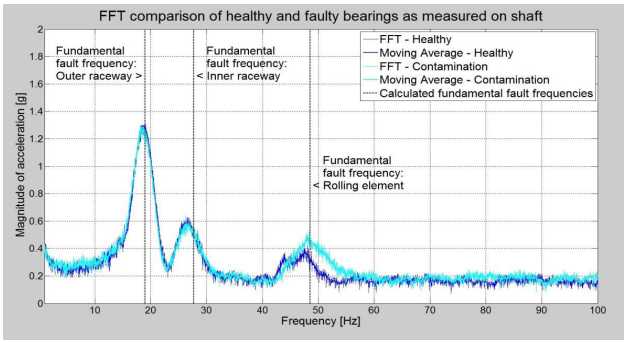

Fig. 15. Shaft-mounted FFT analysis of a contaminated bearing.

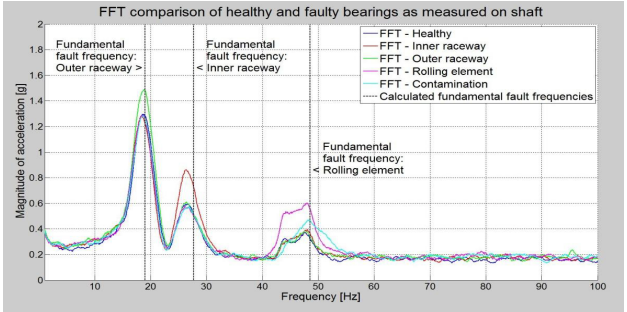

Fig. 16. Averages of shaft bearing conditions.

Despite the fact that only one signal per bearing fault is displayed, 72 data sets were obtained for this case, of which 36 were used for training and the remaining 36 were used to test the identification and classification process. The number of test sets is tabulated in the results table for each case.

Figure 17 depicts how the percentage contribution of each wavelet to the signal was used to normalise the energy levels of the wavelets. Using an intelligent system, the various energy distributions were used to identify and classify bearing faults. Only the first thirteen levels are displayed, as the remaining energy bands are insignificant in comparison to the low-frequency bands. Observably, some frequency bands are dominated by the fundamental frequency present in that frequency range.

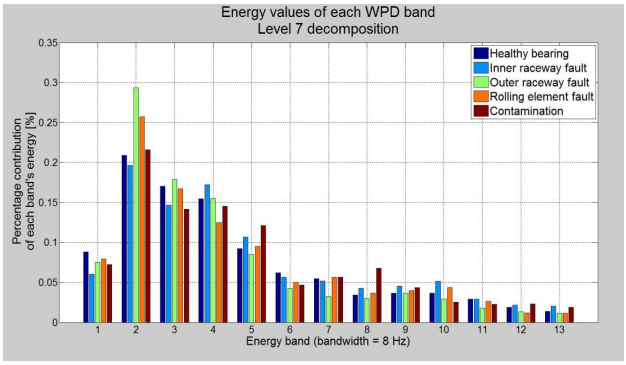

Fig. 17. WPD of shaft bearing defects.

The FFT of a normal bearing signal is displayed in Figure 18. The FFT's moving average is also demonstrated and used. Over the course of all of the trials, we used a simple moving average. The majority of the noise was removed using only the five reference points before and after the data being analyzed.

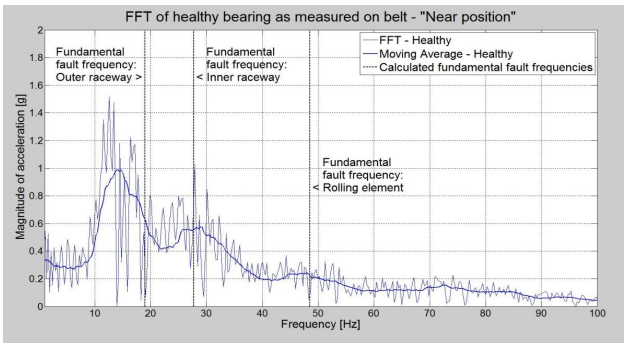

Fig. 18. FFT near a healthy bearing.

Figure 19 shows an inner raceway fault bearing's near FFT. Also included is a healthy bearing's FFT. Moving FFT averages are shown. As expected from previous tests, Figure 19 shows that the faulty bearing had a higher inner raceway fundamental frequency than the healthy bearing. Outer race and rolling element fundamental frequencies changed little. 394 bearing inner raceway fault datasets were recorded. The faulty bearing was replaced with one with an artificial outer raceway fault.

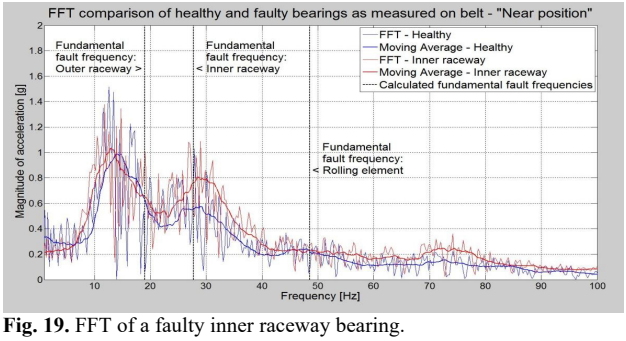

Fig. 19. FFT of a faulty inner raceway bearing.

Figure 20 shows an outer raceway fault bearing's near FFT. Also included is a healthy bearing's FFT. Moving FFT averages are shown. Outer raceway fundamental frequency increased clearly.

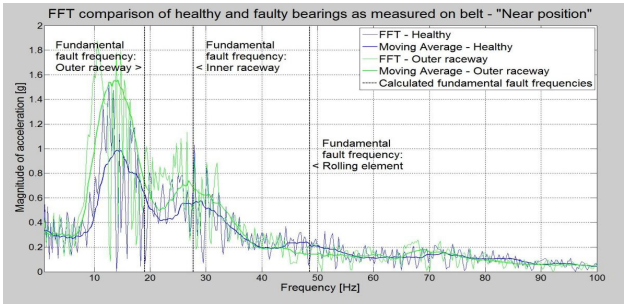

Fig. 20. FFT of a faulty bearing's outer raceway.

Both the outer raceway fundamental frequency and the inner raceway fundamental frequency were augmented. The fundamental frequency of the outer raceway was seen to increase by an order of magnitude. A total of 535 datasets recorded the bearing with an external raceway fault. The faulty bearing was removed and replaced with a bearing with an artificially induced rolling element fault. The five different bearing conditions are shown as moving averages in Figure 21. The frequency spectrum of each bearing condition clearly has a different shape, and this difference was used to categories the bearing states.

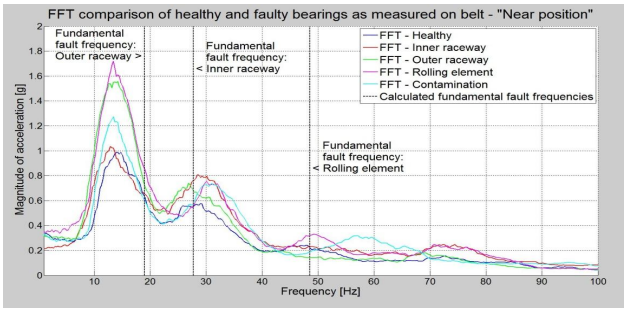

Fig. 21. Near-bearing moving averages of bearing conditions.

9. Conclusion And Future Recommendations

Unfortunately, the high cost of a reliable conveyor idler monitoring system makes it impractical for many establishments. There are a number of methods for keeping tabs on or inspecting idlers, but one that works well with an online system is the utilization of vibrations. With this system, we can check products thoroughly while spending less on labour. Vibrations were found to be a highly accurate method of detecting damaged idlers when the accelerometer was placed on top of the revolving belt. Although installing one accelerometer for every three or more idlers will help, a large number of accelerometers will still be needed to track all of the conveyor's tremors.

It was investigated if an accelerometer could be fastened to the moving belt rather than each individual idler bearing. The accelerometer measured the vibration levels of each idler as it travelled the length of the conveyor. The tests demonstrated that an accelerometer, irrespective of its position or payload, could be used to effectively detect and classify idler bearing failures. The defective bearing was identified by the custom data acquisition system that was mounted on the moving conveyor belt. A support vector machine and wavelet package decomposition were used in

the early stages of the process to achieve this level of accuracy.

The results indicate that the in-belt monitor can identify a faulty bearing long before the bearing completely fails. That way, we can identify all the defective bearings, plan for their suitable alternative in advance of an upcoming outage, and solve the issue inside one fell swoop. As a result, the conveyor feed will be interrupted for shorter periods of time than usual, and a solitary, longer outage can be planned all through which all broken or impending damaged bearings can be supplanted. It is impossible to predict what long the damaged bearings will remain ineffective using our current method of monitoring. This is a fantastic improvement that will greatly aid in contingency planning during power outages.

As future recommendations, more investigation is required into the non-linearity in the on-belt measurement device and the effect of belt speed different variants on evaluated fundamental frequencies. The sensor's resonant frequency is obviously altered due to the system's non-linearity. Understanding the dynamics of the system is crucial for analyzing the based on the measured signals and discovering why the anticipation frequencies show up at subharmonic or super harmonic questions and issues when the sensor is positioned on top of the belt need to investigated further.

Acknowledgment

The authors would like to extend their gratitude to Auckland University of Technology, Auckland, New Zealand, which provided financial and testbed support for this research.

References

1. Al-Ahmar, M. A. (2019). Estimation of Induction Motor Model Parameters-Case Study. L. ERJ. Engineering Research Journa, (pp. 42(3), 177-182).
2. Al-Hashedi, K. G. (2021). Financial fraud detection applying data mining techniques: A comprehensive review from 2009 to 2019. Computer Science Review,, (pp. 40, 100402).
3. Ayhan, B. C. (2005). Multiple signature processing-based fault detection schemes for broken rotor bar in induction motors. Transactions on Energy Conversion (pp. 20(2), 336-343). IEEE .
4. Bari, A. J. (2017). Fault Tolerant Industrial Wireless Sensor Networks. In Industrial Wireless Sensor Networks. (pp. (pp. 137-160)). CRC Press.
5. Bindu, S. &. (2018). Detection of Static Air-Gap Eccentricity in Three-Phase Squirrel Cage Induction Motor Through Stator Current and Vibration Analysis. Advances in Power Systems and Energy Management (pp. (pp. 511-518).). Singapore.: Springer, .
6. Boudane, F. &. (2017). (2017, December). Variable neighborhood search for automatic density-based clustering. In 2017 . International Conference on Mathematics and Information Technology (ICMIT) (pp. (pp. 141-147).). IEEE.
7. Bruno, R. &. (2015). Spectral analysis of magnetic fluctuations at proton scales from fast to slow solar wind. The Astrophysical Journal Letters, (pp. 811(2), L17).
8. Chen, X. &. (2010, March). Notice of Retraction: Gaussian Research of Turbine Faults Diagnosis Base on Mixture Models. In 2010 Asia-Pacific Power and Energy Engineering Conference. (pp. (pp. 1-5)). IEEE.
9. Cruz, S. M. (2008). A new model-based technique for the diagnosis of rotor faults in RFOC induction motor drives. Transactions on Industrial Electronics (pp. 55(12), 4218-4228.). IEEE.
10. Fu, J. X. (2019, November). Study on Simulation of Asynchronous Motor Rotor Broken Bar Fault. Chinese Automation Congress (CAC) (pp. pp. 2894-2897). IEEE.
11. Hassan, O. E. (2018). Induction motor broken rotor bar fault detection techniques based on fault signature analysis–a review. . IET Electric Power Applications, , (pp. 12(7), 895-907.).
12. Hassanzadeh, M. F. (2019). A new analytical technique for analysis and detection of air-gap eccentricity fault in surface-mounted permanent-magnet machines. . International Transactions on Electrical Energy Systems,, (pp. 29(3), e2764.).
13. Herndler, B. B. (2011). Considerations for improving the non-intrusive efficiency estimation of induction machines using the air gap torque method. International Electric Machines & Drives Conference (IEMDC) (pp. 1516-1521). IEEE.
14. Hou, L. &. ((2012).). Novel industrial wireless sensor networks for machine condition monitoring and fault diagnosis. IEEE transactions on instrumentation and measurement, (pp. 61(10), 2787-2798.). IEEE .
15. Hui, K. H.-O. (2017). Dempster-Shafer evidence theory for multi-bearing faults diagnosis. Engineering Applications of Artificial Intelligence., (pp. 57, 160-170.).
16. Ishikawa, T. S. (2013). Analysis and failure diagnosis of squirrel-cage induction motor with broken rotor bars and end rings. IEEJ Journal of Industry Applications, (pp. 2(6), 292-297.).
17. Jankowska, K. &. (2022). Design and Analysis of Current Sensor Fault Detection Mechanisms for PMSM Drives Based on Neural Networks. Designs., (pp. 6(1), 18.).
18. Krishna, M. S. (2013). Neural network for the diagnosis of rotor broken faults of induction motors using MCSA. 7th International Conference on Intelligent Systems and Control (ISCO) (pp. pp. 133-137). IEEE.
19. Luo, H. H. ((2019).). A dual-tree complex wavelet enhanced convolutional LSTM neural network for structural health monitoring of automotive suspension. Measurement, ., (pp. 137, 14-27.).
20. Luong, P. &. (2020). Smart sensor-based synergistic analysis for rotor bar fault detection of induction motors. ASME Transactions on Mechatronics (pp. 25(2), 1067-1075.). IEEE.
21. Meshgin-Kelk, H. (2017). Modeling of Electric Machines Using Magnetic Equivalent Circuit Method. book chapter (Electric Machines. Modeling, Condition Monitoring, and Fault Diagnosis), (pp. 47-80.).
22. Misra, R. &. (2015). Fuzzy logic based rotor health index of induction motor. International Journal of Emerging Electric Power Systems., (pp. 443-449, 16(5)).
23. Nandi, S. (2017). Fault Diagnosis of Electric Machines Using Techniques Based on Frequency Domain. Electric Machines: Modeling, Condition Monitoring, and Fault Diagnosis, ., (p. 99).
24. Navarro, J. M.-E.-C. (2020). Sound levels forecasting in an acoustic sensor network using a deep neural network. Sensors, (pp. 20(3), 903.).
25. Pandarakone, S. E. (2018). Deep neural network based bearing fault diagnosis of induction motor using fast Fourier transform analysis. . energy conversion congress and exposition (ECCE) (p. 32). IEEE.
26. Pereira, R. A. (2009). Improved fault location on distribution feeders based on matching during-fault voltage sags. . Transactions on Power Delivery, (pp. 24(2), 852-862.). IEEE.
27. Taïb, Z. M. (n.d.). Motor Current Demodulation Analysis applied with Neural Networks and Genetic Algorithms for Rotor Bar Faults Diagnosis.
28. Thomson, W. T. (2016). Motor current signature analysis for induction motors. Current signature analysis for condition monitoring of cage induction motors: Industrial application and case histories, ., (pp. 1-37).
29. Tsypkin, M. (2017). Induction motor condition monitoring: Vibration analysis technique—diagnosis of electromagnetic anomalies. AUTOTESTCON (pp. 1-7). IEEE.

30. Tyagi, S. &. (2017). A simple continuous wavelet transform method for detection of rolling element bearing faults and its comparison with envelope detection. Int. J. Sci. Res, 6, (pp. 1033-1040.).
31. Xu, J. Z. (2020). Modeling and Analysis of Temperature Field of Permanent Magnet Synchronous Motor Considering High Frequency Magnetic Field Characteristics. SAE Technical Paper., (pp. No. 2020-01-0457).
32. Yassa, N. R. (2019). Motor current signature analysis for the air gap eccentricity detection in the squirrel cage induction machines. (pp. 162, 251-262.). Energy Procedia.
33. Yetgin, A. G. (2019). Effects of induction motor end ring faults on motor performance. Experimental results. Engineering Failure Analysis, (pp. 96, 374-383.).
34.